Rare Met. (2020) 39(11):1279–1287
https://doi.org/10.1007/s12598-018-1172-1

RARE METALS
www.editorialmanager.com/rmet

Solidification behavior and elimination of undissolved Al_2CuMg phase during homogenization in Ce-modified Al–Zn–Mg–Cu alloy

Xin-Xiang Yu*, Jie Sun, Zhu-Tie Li, Han Dai, Hong-Jie Fang, Jun-Feng Zhao, Deng-Feng Yin

Received: 4 October 2017 / Revised: 28 December 2017 / Accepted: 9 October 2018 / Published online: 3 December 2018

Abstract The solidification behavior and intermetallic phase evolution during homogenization annealing of an Al–Zn–Mg–Cu alloy with 0.12 wt% Ce addition were examined. The residual Al_2CuMg phase is completely dissolved after homogenization and is replaced by a large number of dispersed micro/nanoscaled AlCuCe enrichment phases within Al matrix. This change occurs because of the formation of a large number of finer lamellar eutectic network structures which are more easily dissolved into Al matrix during the homogenization process. In addition, the trapping of Cu atoms in the stable AlCuCe phase also prevents the formation of Al_2CuMg phase, leading to the complete dissolution of Al_2CuMg phase in the Al–Zn–Mg–Cu alloy. The grain refinement behavior in Al alloy with Ce addition is similar to that in alloys with the addition of Sc, because of the formation of primary Ce-enriched $Al_{11}Ce_3$ phase as the nucleation agent of α(Al) during solidification.

Keywords Al–Zn–Mg–Cu alloy; Al_2CuMg phase; Homogenization; Grain refinement

1 Introduction

High-alloyed Al–Zn–Mg–Cu alloys are extensively used in aerospace and military industries because of their high specific strength, stress corrosion cracking resistance and fracture toughness [1, 2]. However, coarse intermetallic particles form in Al–Zn–Mg–Cu alloys with higher alloying element contents [3, 4]. The residual bulky intermetallic compounds (> 1 μm) typically first result in brittle fracture during deformation, which may be the source of crack initiation for Al–Zn–Mg–Cu alloys. Thus, these coarse residual phases can damage the toughness, fatigue properties [5] and corrosion properties of Al–Zn–Mg–Cu alloys [6]. In general, these large soluble non-equilibrium solidification intermetallic phases can be effectively eliminated through their re-dissolution into the matrix during homogenization [7]. However, the high-temperature stable Al_2CuMg phase hardly dissolves into the matrix during homogenization [8]. A series of efforts have been made to remove this Al_2CuMg phase, Deng et al. [9] developed new multi-step ultrahigh temperature homogenization technology to eliminate the Al_2CuMg residual phase. Liu et al. [10] reported that the Al_2CuMg phase was not observed after homogenization and was instead replaced by many residual AlZnMgCu phases, in an Al–Zn–Mg–Cu alloy with special high Zn content. Nevertheless, the over-burnt phenomenon may easily occur in actual industrial applications of Al–Zn–Mg–Cu alloys because of the ultrahigh temperature homogenization, and the presence of many residual AlZnMgCu phases in Al–Zn–Mg–Cu alloys with higher Zn content after homogenization may still worsen the performance of these alloys.

Zhang et al. [11] added Ce to an Al–18 wt% Si alloy and observed that the morphology of the primary Si and eutectic Si could be effectively modified from fibrous to lamellar shape. There have also been many reports on the effect of Ce on the morphology of intermetallic compounds of 7XXX series aluminum alloys, e.g., a refined dendritic structure with the precipitate morphology changing from

X.-X. Yu*, J. Sun, H. Dai, H.-J. Fang, J.-F. Zhao, D.-F. Yin
School of Engineering, Yantai Nanshan University, Yantai 265713, China
e-mail: xxyucn@qq.com

X.-X. Yu, Z.-T. Li, H. Dai
Testing and Analysis Center, Shandong Nanshan Aluminum Co. Ltd., Yantai 264006, China

spherical to needle shape in 7055Al alloy [12] and a refined eutectic microstructure in Al–6.7Zn–2.6Mg–2.6Cu (wt%) alloy [13]. The refinement or change of the morphology of the eutectic phase in as-cast alloys can affect the diffusion of segregation elements to the matrix during homogenization [10]. Therefore, the segregation elements, particularly Cu with its lower diffusion coefficient [8], in an appropriate eutectic phase morphology might also be favorably dissolved into the matrix during homogenization annealing. Meanwhile, the reason for adding 0.12 wt% Ce is that the addition of Ce to Al–Zn–Mg–Cu alloy increases the formation and stability of the AlCuCe enrichment phase [14, 15], which would effectively prevent the formation of the high-temperature stable Cu-containing Al_2CuMg phases.

In binary Al–Sc hypereutectic alloys with Sc contents above 0.55 wt%, the first solidification phase to form during solidification is Al_3Sc, which precipitates as fine particles in the liquid. The $L1_2$ crystal structure of these particles and their low lattice parameter mismatch with Al (1.6%) possibly make them effective nucleating agents [16]. However, the use of Sc is not cost-effective, which restricts its wide application. Similar to Sc, the rare-earth element Ce exhibits a liquid → α(Al)-$Al_{11}Ce_3$ eutectic reaction during solidification [17]. The Ce addition has been reported to affect the grain size of Al–Cu–Mg–Mn–Ag alloys [18] and refine the as-cast grains in Al–6.7Zn–2.6Mg–2.6Cu (wt%) alloy [13]. Nevertheless, it is difficult to find primary particles ($Al_{11}Ce_3$) that can act as heterogeneous nucleants at the center of Al grains for alloys with a rare-earth element addition except for Sc. Thus, it is generally accepted that grain refinement in other rare-earth containing alloys is not the result of the nucleation initiation of the first Al_3Re phase because their lattice parameter mismatch is very large compared with Al [19].

Herein, the rare-earth element Ce was introduced to study its effect on the solidification behavior and elimination of Al_2CuMg phase during homogenization in a high-alloyed Al–Zn–Mg–Cu alloy. The morphological and compositional changes of the eutectic phase in Ce-free and Ce-containing Al–Zn–Mg–Cu alloys after casting and subsequent annealing were investigated. Obvious grain refinement and dissolution of the Al_2CuMg phase are observed during homogenization in the Al–Zn–Mg–Cu alloy with 0.12 wt% Ce addition. In addition, the main mechanisms responsible for the remarkable grain refinement during solidification and thorough elimination of the high-temperature residual Al_2CuMg phase during homogenization in the Al–Zn–Mg–Cu alloy were proposed. This work provides new insight to aid in improving the performance of high-alloyed Al–Zn–Mg–Cu alloys through Ce addition.

2 Experimental

The experimental alloys were melted by induction heating and then cast into Cu molds to produce billets with 190 mm in length, 130 mm in width and 24 mm in thickness. After the alloy (American series 7136 alloy) or the addition of 0.12 wt% Ce being remelted directly, the measured composition is shown in Table 1, by means of inductively coupled plasma-atomic emission spectrometry (ICP-AES) method on BAIRD PS-6. The billets were homogenized at 440 °C for 12 h and 470 °C for 32 h, followed by air cooling to room temperature. The homogenization treatments were performed in a salt bath furnace with an accuracy of ± 2 K. Differential scanning calorimeter (DSC, METTLER TOLEDO DSC1/700) was performed at a heating rate of 10 $K \cdot min^{-1}$ to determine the melting points of the intermetallic phases. Phase identification was performed using X-ray diffractometer (XRD, Rigaku D/max-2400) with Cu $K\alpha_1$ radiation. A combination of optical microscopy (OM, ZEISS Image M2m), scanning electron microscopy (SEM, Nova-Nano SEM450) and electron probe microanalysis (EPMA, JEOL JXA-8230, 20 kV) was used to characterize the as-cast and homogenized microstructures. SEM, in the backscattered electron (BSE) imaging mode, was performed using a scanning electron microscopy attached to EPMA instrument, operating at 20 kV. A quantitative X-ray wavelength-dispersive spectroscopy (WDS) system attached to EPMA instrument was used to analyze the chemistry of the intermetallic phases present in the as-cast and homogenized microstructures. Scanning transmission electron microscopy (STEM) analysis and elemental mapping using energy-dispersive X-ray spectroscopy (EDS) measurements were performed on a JEOL-2100F system.

3 Results

3.1 Microstructure of as-cast alloys

Figure 1 presents OM images of as-cast Ce-free and Ce-containing Al–Zn–Mg–Cu alloys. The addition of 0.12 wt% Ce clearly results in efficient grain refinement. The average grain size of the as-cast alloys is refined from ~ 300 μm in Ce-free alloy to 80 μm in Ce-containing

Table 1 Chemical compositions of investigated alloys (wt%)

Alloys	Zn	Mg	Cu	Ce	Al
Al–Zn–Mg–Cu	8.46	1.95	2.44	–	Bal.
Al–Zn–Mg–Cu–0.12Ce	8.48	1.94	2.45	0.12	Bal.

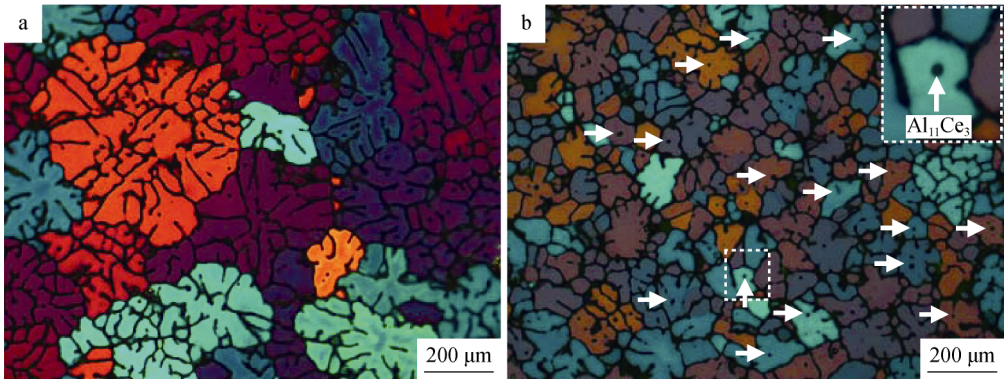

Fig. 1 OM images of as-cast alloys: **a** Al–Zn–Mg–Cu and **b** Al–Zn–Mg–Cu–0.12Ce

alloy. Figure 1b also reveals that as refinement occurs, there is a complete lack of a dendritic substructure within the majority of the fine equiaxed grains which appear to have grown with a spherical front without exhibiting any internal phase or solute partitioning condition. However, a number of primary intermetallic particles are distributed within the fine equiaxed grains, as indicated by arrow in Fig. 1b.

Figure 2 presents SEM images of as-cast Ce-free and Ce-containing Al–Zn–Mg–Cu alloys. Eutectic solidified structures of Al–Zn–Mg–Cu and Al–Zn–Mg–Cu–0.12Ce alloys can be clearly observed in the enlarged images, respectively. A large number of finer lamellar eutectic network structures form during solidification in the Ce-modified Al–Zn–Mg–Cu alloy. Because of the substantial differences in brightness and morphology of the intermetallic microstructures in the two alloys, the eutectic phases can be classified into four types, marked as A, B, C and D. The corresponding quantitative WDS analysis results are presented in Table 2. The analysis reveals that the gray continuous phase (Area A in Fig. 2a) is AlZnMgCu phase and the gray lamellar eutectic structure phase (Areas B and C in Fig. 2) is a mixture of α(Al) and AlZnMgCu phases. Only Al, Cu and Ce are detected by WDS in the white phase (Area D in Fig. 2b), suggesting that it might be Ce segregated within Al_2Cu phase [20].

As observed in Figs. 3 and 4, the main elements Zn, Mg and Cu are largely enriched in the dendritic boundary, and the concentration of the elements gradually decreases upon moving from the dendritic boundary to the interior. Cu and Ce tend to be concentrated together with an extreme deficiency of Mg in $Al_2(Cu, Ce)$ phase, as observed in Fig. 4. Another type of only Ce-enriched phase with a size of 18 μm may be the primary $Al_{11}Ce_3$ particles that normally

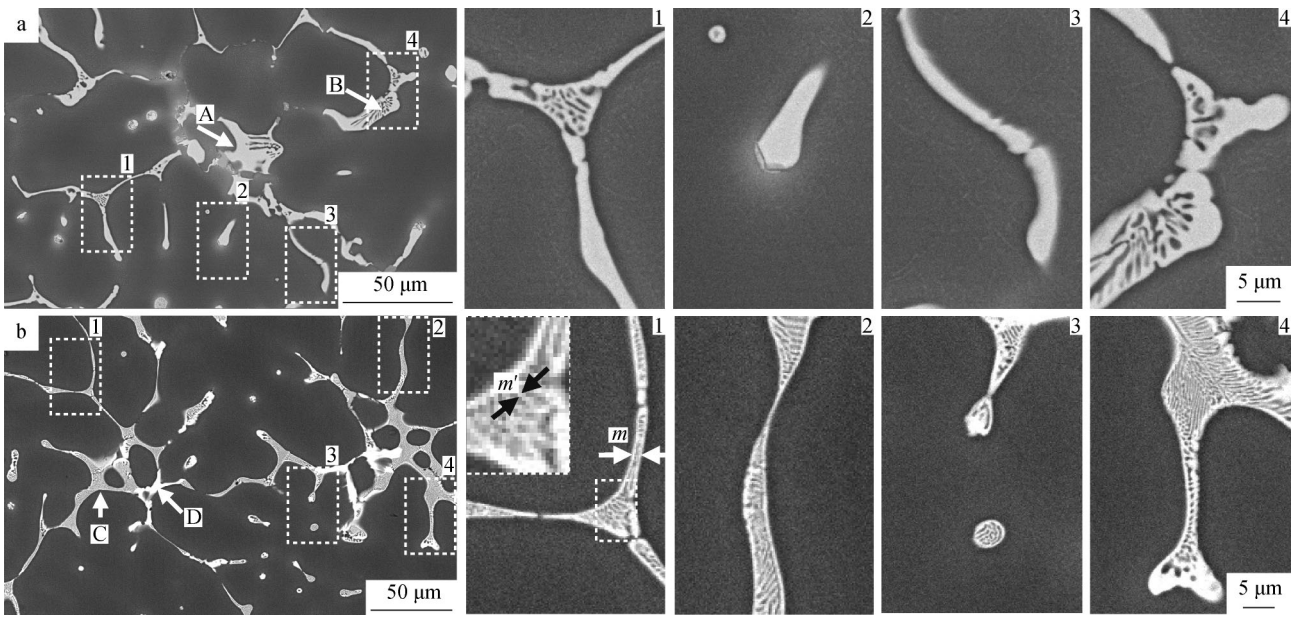

Fig. 2 BSE images and corresponding magnified images of rectangular boxes of as-cast alloys: **a** Al–Zn–Mg–Cu and **b** Al–Zn–Mg–Cu–0.12Ce

Table 2 Chemical composition of intermetallic phases in Fig. 2 (wt%)

Items	Al	Zn	Mg	Cu	Ce	Phases
A	27.20	28.17	31.57	13.06	–	$Mg(Zn, Al, Cu)_2$
B	54.80	19.66	17.32	8.22	–	$\alpha(Al) + Mg(Zn, Al, Cu)_2$
C	62.63	12.88	16.93	7.56	–	$\alpha(Al) + Mg(Zn, Al, Cu)_2$
D	60.64	7.51	–	22.96	6.05	$Al_2(Cu, Ce)$

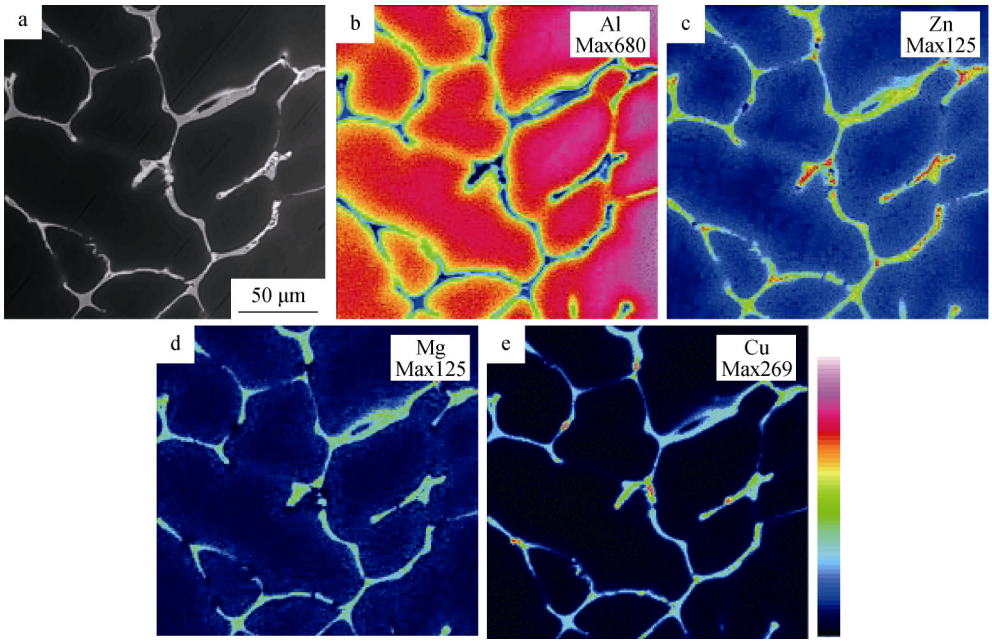

Fig. 3 SEM images of microstructure and distribution of main elements in as-cast Al–Zn–Mg–Cu alloy: **a** BSE image; elemental mappings of **b** Al, **c** Zn, **d** Mg and **e** Cu (numbers in top right corner being relative concentration of elements)

form in hypereutectic Al–Ce alloy (encircle in Fig. 4a). $Al_{11}Ce_3$ particles have a typical square shape and a size of ~ 20 μm, similar to the characteristics of primary Al_3Sc intermetallic particles [16].

3.2 Microstructure of homogenized alloys

The microstructures of Ce-free and Ce-containing Al–Zn–Mg–Cu alloys after homogenization annealing are shown in Fig. 5. The dissolution of solidification phase occurs within the dendrite cell and along the dendrite boundary after homogenization at 440 °C for 12 h and 470 °C for 32 h. Meanwhile, a new gray intermetallic phase forms, as observed in Fig. 5a. The chemical compositions of the gray phase marked in Fig. 5a are 60.94 at% Al, 19.27 at% Cu and 19.79 at% Mg, as measured by quantitative WDS analysis. The new gray intermetallic phases are thought to be the undissolved Al_2CuMg phase because of the Cu to Mg ratio close to 1:1 in this phase. After Ce addition, Al_2CuMg phase completely dissolves into the matrix, and only a few microscale AlCuCe intermetallic particles and $Al_{11}Ce_3$ intermetallic particles (square in shape and 16–23 μm in size) are detected, as shown in Fig. 5b. Inside Al matrix, nanoscaled AlCuCe enrichment phases (indicated by arrow in Fig. 5c) in the homogenized Al–Zn–Mg–Cu–0.12Ce alloy are observed. The size of nanoscaled AlCuCe enrichment phases is 200–500 nm, and the particles are marked in Fig. 5c. The elemental distributions of Al, Cu, and Ce in these particles are intensively segregated together, as demonstrated in the mapping results in Fig. 5d. The large number of micro/nanoscale AlCuCe particles distributed within Al matrix in the Ce-modified Al–Zn–Mg–Cu alloy leads to considerable Cu atom trapping and hinders further formation of Al_2CuMg phase during homogenization.

Figure 6a, b presents DSC plots of Al–Zn–Mg–Cu and Al–Zn–Mg–Cu–0.12Ce alloys in the as-cast and homogenized states. The first endothermic peak (Peak A) at 478.4 °C is observed in both alloys. After homogenization, Peak A is nearly eliminated and another endothermic peak

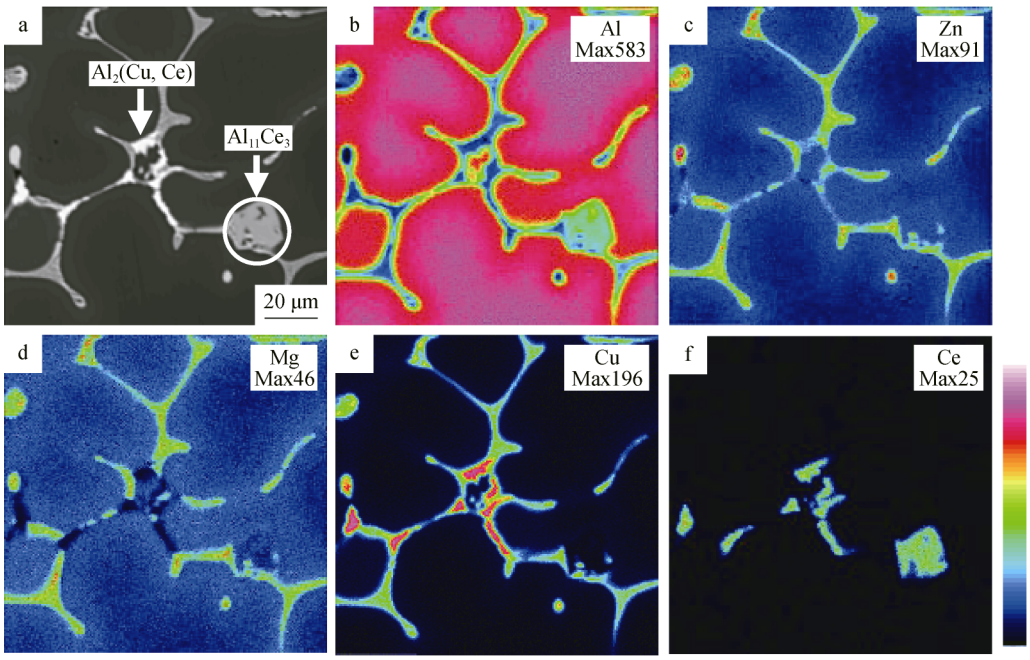

Fig. 4 SEM images of microstructure and distribution of main elements in as-cast Al–Zn–Mg–Cu–0.12Ce alloy: **a** BSE image; elemental mappings of **b** Al, **c** Zn, **d** Mg, **e** Cu and **f** Ce

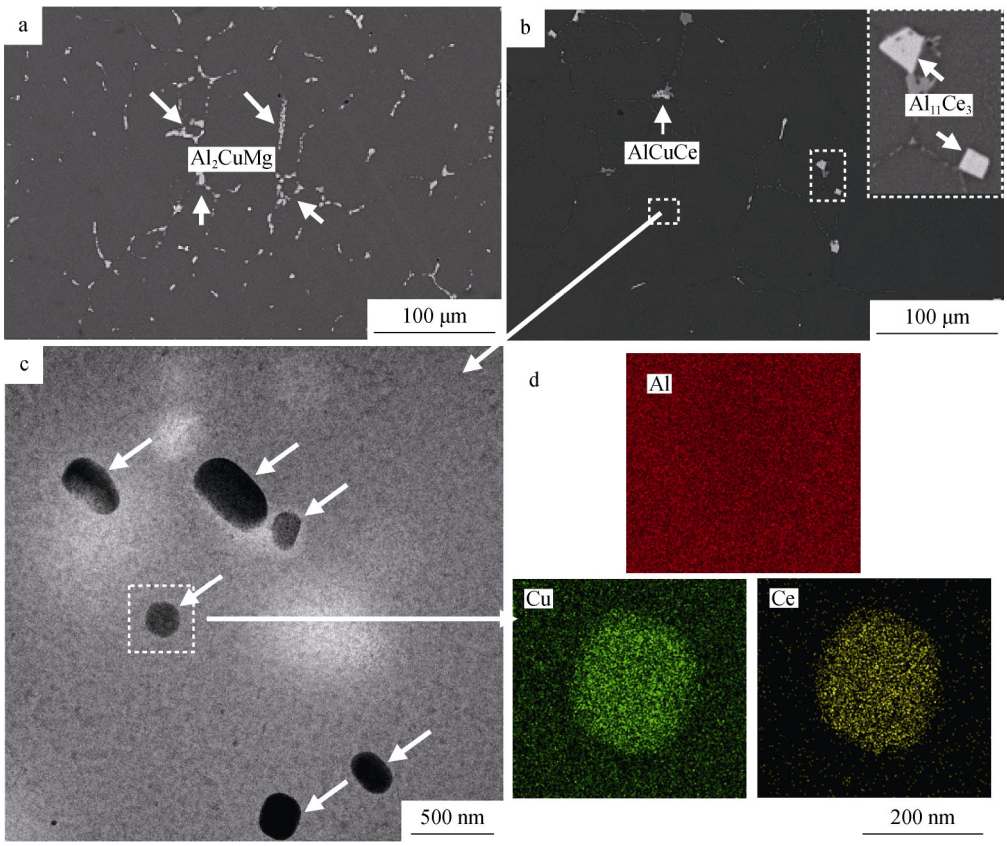

Fig. 5 BSE images of homogenized alloys: **a** Al–Zn–Mg–Cu and **b** Al–Zn–Mg–Cu–0.12Ce; **c** STEM image of AlCuCe particles; **d** elemental mapping of Al, Cu and Ce in particle in square box in **c**

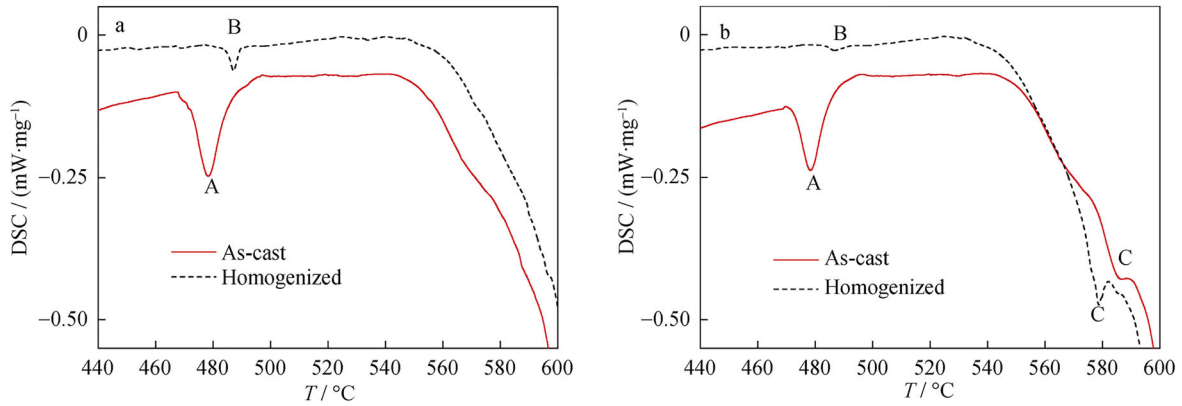

Fig. 6 DSC curves of **a** Al–Zn–Mg–Cu and **b** Al–Zn–Mg–Cu–0.12Ce alloys

appears at 486.9 °C (Peak B) in both alloys. Peak B is attributed to the dissolution of Al_2CuMg phase [9]. However, the intensity of Peak B in Fig. 6b is much less than that in Fig. 6a, indicating that only a small amount of undissolved Al_2CuMg phases are formed in Al–Zn–Mg–Cu alloy with the addition of Ce. An additional endothermic peak appears at 578.9 °C (Peak C) in the as-cast Ce-containing alloy, as observed in Fig. 6b. After homogenization, Peak C shifts to even higher temperature (586.9 °C). Based on previous microstructural observations (Figs. 2b, 5b) and results in Ref. [21], the endothermic Peak C is attributed mainly to the melting of Ce-enriched phases, i.e., $Al_2(Cu, Ce)$ phases in the as-cast state and AlCuCe phase in homogenized state. The Ce-containing AlCuCe phase clearly exhibits an increased resistance to melting compared with Al_2Cu phase, as demonstrated by DSC melting peak of AlCuCe phase appearing above 578 °C, whereas that of Al_2Cu phase generally appears at 532 °C [5]. These AlCuCe phases with high-temperature stability are hardly re-dissolved during homogenization; thus, AlCuCe phase can trap many Cu atoms and effectively inhibits further formation of Al_2CuMg phase during homogenization.

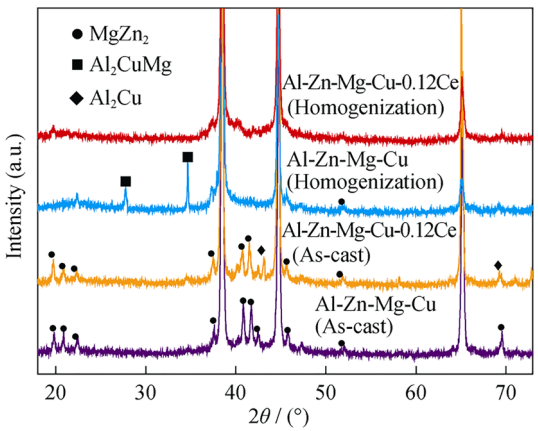

Fig. 7 XRD patterns of Al–Zn–Mg–Cu and Al–Zn–Mg–Cu–0.12Ce alloys

XRD patterns of Ce-free and Ce-containing alloys in as-cast and homogenized states are presented in Fig. 7. XRD peaks that originate from $MgZn_2$ ($Mg(Zn, Al, Cu)_2$) phase could be distinguished in both alloys in the as-cast state. After homogenization, $Mg(Zn, Al, Cu)_2$ phase is nearly eliminated, and XRD peaks originating from Al_2CuMg phase are distinguished only in Ce-free alloy. Therefore, the elimination of Al_2CuMg phase during homogenization in Ce-containing alloy is also supported by XRD results. However, the peak of Ce-containing $Al_2(Cu, Ce)$ phase is also observed in as-cast Al–Zn–Mg–Cu–0.12Ce alloy. The AlCuCe phase is not detected after homogenization because of its nanoscale size, which is the experimental limit for X-ray diffractometer used [20]. Based on above analysis, it should be noted that these nanoscaled AlCuCe dispersoids with high-temperature stability might effectively prevent recrystallization during subsequent thermo-mechanical processing by pinning grain and subgrain boundaries.

4 Discussion

4.1 Effect of Ce addition on grain refinement of as-cast Al–Zn–Mg–Cu alloy

The refinement of as-cast grain size of the high-alloyed Al–Zn–Mg–Cu alloy is far greater than that achieved using conventional grain refiners [22] and other rare-earth elements, e.g., Er [19] and Yb [23] in Al alloys. There is grain refinement with the addition of 0.12 wt% Ce accompanied by a change in the growth morphology. In detail, the large unrefined grains with dendritic growth transform into the fine spherical grains with divorced eutectic structure, which occurs on the grain boundaries in the refined casting (Fig. 1). Similar refinement phenomena have only been observed in Al alloys with Sc addition [16]. For Sc additions less than the eutectic composition of 0.55 wt% Sc, an

unrefined large grain size is observed, whereas for Sc contents above 0.55 wt%, a dramatic reduction in grain size is observed. Analogously, Al–Ce binary phase diagram shows that a eutectic reaction occurs at 650 °C with a composition of 0.05 wt% Ce, resulting in the formation of $Al_{11}Ce_3$ intermetallic phase [24]. For the experimental alloy in this study, the addition of 0.12 wt% Ce (which is greater than the eutectic composition of 0.05 wt% Ce) results in a remarkable refinement of the grain size of aluminum casting (from ~ 300 to 80 μm), due to the formation of primary $Al_{11}Ce_3$ intermetallic phase during solidification (Figs. 1b, 2b, 4b). Interesting behavior is also observed when the substructures of the refined cast grains were examined in detail. In the Ce-free alloy, a typical dendritic substructure is observed (Fig. 1a). The first phase to solidify is clearly α(Al), as expected from phase diagram; this phase nucleates predominantly on the mold wall and grows inwards to form large columnar grains. The liquid ahead of the solidification front eventually becomes sufficiently supercooled to allow a region of equiaxed grains to form. In fact, the alloys in this study contain a large amount of alloying elements, resulting in the solute on the front of the solid/liquid interface being enriched during solidification. Thus, the actual temperature in front of the interface is lower than the solidification temperature determined by the solute distribution, which causes a large undercooling during solidification. Therefore, a large dendritic network is observed in the crystal cell in the Ce-free Al–Zn–Mg–Cu alloy. Conversely, in the Ce-containing alloy, as refinement occurs, there is a complete lack of a dendritic substructure within a few of the refine equiaxed grains, which appear to have grown with a spherical front exhibiting no solute partitioning except for a large number of primary internal intermetallic particles distributed within the fine equiaxed grains (Fig. 1b). This exceptional grain refinement could be attributed to the formation of intermetallic particles of $Al_{11}Ce_3$ phase in the melt, which may have acted as nucleation sites for the remaining α(Al) to grow outwards from the primary $Al_{11}Ce_3$ particle on which α(Al) is nucleated. This behavior is typical of that observed for a "divorced eutectic" [16] and is consistent with the difficulty of coupled growth, when the content of one phase is very small because of the dilute nature of the eutectic composition and when the growth kinetics of the $Al_{11}Ce_3$ phase is slow relative to that of α(Al). Nevertheless, the formation of a divorced eutectic would also require very efficient nucleation of α(Al) on the primary $Al_{11}Ce_3$ particle, as on the primary Al_3Sc. It is apparent that the matching of the crystal structure and lattice parameter of $Al_{11}Ce_3$ phase to those of α(Al) is the key influencing factor. The nucleation of α(Al) on one of the crystal faces of the primary phase $Al_{11}Ce_3$ in the melt must be very efficient upon solidification. Fortunately, the $Al_{11}Ce_3$ phase has an orthorhombic crystal structure with lattice parameters of a = 0.4389 nm, b = 1.3025 nm and c = 1.0092 nm, and α(Al) has a fcc crystal structure with a lattice parameter of a = 0.40496 nm [25]. Thus, nucleation of α(Al) on one of the crystal faces of the primary phase $Al_{11}Ce_3$ would be very efficient.

4.2 Effect of Ce addition on intermetallic phase morphology during solidification

$Mg(Zn, Al, Cu)_2$ solidification phase is formed in Al–Zn–Mg–Cu alloy when Zn/Mg mass ratio is higher than 2.2 [10]. The Zn/Mg mass ratio is ~ 4.34 or 4.37 in the alloys in the current work; thus, the main phases of the as-cast materials are α(Al) and $Mg(Zn, Al, Cu)_2$ (Fig. 2b). It is well known that Al and Cu will substitute for Zn at the lattice position of Zn in the $MgZn_2$ phase with the formation of $Mg(Zn, Al, Cu)_2$; thus, the fraction of $Mg(Zn, Al, Cu)_2$ is determined by Mg content [26]. Cu and Ce tend to be concentrated together at location with extremely Mg deficiencies, as observed for the Ce-containing alloy (Fig. 4). Therefore, the fraction of $Mg(Zn, Al, Cu)_2$ in the current alloys is not affected by Ce addition. The effect of Mg/Cu mass ratio and Zn content on $Mg(Zn, Al, Cu)_2$ phase after casting are summarized in Table 3 [8, 27–32]. The $Mg(Zn, Al, Cu)_2$ phase morphology is significantly affected by Mg/Cu mass ratio. The eutectic transition from residual liquid to lamellar eutectic structured $Mg(Zn, Al, Cu)_2$ phases occurs if Cu content of the residual liquid is sufficiently lower (Mg/Cu mass ratio > 1.1). After the precipitation of crystals of the aluminum solid solution (α(Al)) in the Al–Zn–Mg–Cu alloy begins, the solutes Zn, Mg and Cu are simultaneously diffused to the liquid at the front of solid/liquid interface. Cu atoms are more prone to moving into the residual liquid, whereas Zn and Mg are normally in the form of solid solution (Figs. 3, 4). Therefore, the concentration of the solute Cu in the residual liquid is the key factor determining the final morphology of the $Mg(Zn, Al, Cu)_2$ phase. By combination of the solidification phase observation (Fig. 2b) and DSC analysis of Al–Zn–Mg–Cu–0.12Ce alloy (Fig. 6b), it is apparent that a Ce-containing $Al_2(Cu, Ce)$ phase forms easily during solidification. Thus, similar to that of Sc-containing Al–Zn–Mg–Cu alloy, crystallization of Ce-containing Al–Zn–Mg–Cu alloy begins with the precipitation of crystals in the aluminum solid solution followed by the formation of the binary "divorced" eutectic α(Al) + $Al_{11}Ce_3$. After most of the crystallizations of the "divorced" eutectic, crystallization of the binary eutectic α(Al) + $Al_2(Cu, Ce)$ first occurs followed by solidification of the alloys, resulting in the formation of α(Al) and $Mg(Zn, Al, Cu)_2$ with lamellar eutectic structures. This result is attributed to the large number of Cu atoms trapped in the $Al_2(Cu, Ce)$ phase;

Table 3 Effect of Cu/Mg ratio on Mg(Zn, Al, Cu)$_2$ phase morphology after casting

Alloys	Content/wt%			Mg/Cu mass ratio	Rare-earth element content/wt%	Fine lamellar eutectic structure	References
	Zn	Mg	Cu				
7449	8.59	2.28	1.90	1.20	–	Yes	[27]
7056	9.42	2.01	1.63	1.23	–	Yes	[27]
7136	8.58	1.95	2.16	0.90	–	No	[27]
7095	9.09	1.78	2.24	0.79	–	No	[27]
–	12.24	3.25	2.46	1.32	–	Yes	[28]
7X50	6.43	2.32	2.08	1.12	–	Yes	[29]
–	8.59	2.00	2.44	0.82	–	No	[30]
–	7.53	1.40	1.57	0.89	0.50Er	Yes	[31]
–	6.31	2.33	1.70	1.37	–	Yes	[8]
–	7.55	1.58	1.39	1.14	–	Yes	[32]
Present work	8.46	1.95	2.44	0.80	–	No	–
	8.48	1.94	2.45	0.79	0.12Ce	Yes	–

therefore, Cu concentration in the final residual liquid is relatively lower, which is favorable for the formation of lamellar eutectic structures during solidification (Fig. 2b). Similar to the finding for a previous reported Er-containing Al–Zn–Mg–Cu alloy (Mg/Cu mass ratio of 0.89) [31], refined lamellar eutectic structures could still be observed in Al–Zn–Mg–Cu alloy with Ce addition, even with Mg/Cu mass ratio $\leq$ 0.80.

4.3 Effect of Ce addition on elimination of undissolved Al_2CuMg phase during homogenization

According to the microstructural analysis (Fig. 5) and corresponding compositional analysis of the residual phases after homogenization, it is concluded that the primary solidification phase Mg(Zn, Al, Cu)$_2$ present in the as-cast microstructure disappears. Meanwhile, a new intermetallic phase Al_2CuMg forms in the Ce-free alloy. However, the residual Al_2CuMg phase is not detected in the Ce-containing alloy. These phenomena can be explained by the diffusion behavior of Cu which has a lower diffusion coefficient than Zn and Mg [8]. According to above analysis, the higher Cu content in the eutectics in Al–Zn–Mg–Cu alloy retards the diffusion process during homogenization heat treatment. Moreover, the higher supersaturation extent of Cu in the Ce-free alloy will provide more Cu solutes to form $A1_2CuMg$ phase and lead to more stable $A1_2CuMg$ particles. Hence, the Ce-free alloy with higher Cu content in the supersaturation solid solution contains more $A1_2CuMg$ particles during homogenization. However, the stable AlCuCe phase in the Ce-containing alloy can trap many Cu atoms and effectively inhibits further formation of the Al_2CuMg phase during homogenization.

In addition, comparison of the morphologies of Mg(Zn, Al, Cu)$_2$ in the two Al–Zn–Mg–Cu alloys reveals that the transition from Mg(Zn, Cu, Al)$_2$ to Al_2CuMg phases may not occur if Cu is more easily dissolved in Al matrix. Therefore, the significant effect of Mg(Zn, Al, Cu)$_2$ phase morphology can possibly be explained by the diffusion behavior of Cu. The effect of the dendritic thickness (m) on the homogenization time (τ_s) can be expressed as follows [10]:

$$\tau_s = am^b \quad (1)$$

where a and b are constants specified by the alloys used. A slight increase in m will lead to a significant increase in the time required for complete homogenization. Although m for the two alloys is almost the same, the dendritic thickness inside the refined network of the eutectic Mg(Zn, Cu, Al)$_2$ of Al–Zn–Mg–Cu–0.12Ce alloy (m') only ranges from 0.2 to 0.4 μm, as observed in Fig. 2d. The phase elimination can be greatly accelerated by decreasing the dendritic thickness. Therefore, Mg(Zn, Al, Cu)$_2$ phase with finer dendritic network structure could be dissolved more rapidly during homogenization. Moreover, Al_2CuMg phase in the Al–Zn–Mg–Cu alloy could be sufficiently eliminated with the addition of Ce.

5 Conclusion

The solidification behavior and intermetallic phase evolution during homogenization annealing of an Al–Zn–Mg–Cu alloy with 0.12 wt% Ce addition were examined. The addition of 0.12 wt% Ce results in clear grain refinement (300–80 μm), which is attributed to efficient α(Al) nucleation on one of the crystal faces of the $Al_{11}Ce_3$ primary phase. A large number of finer lamellar eutectic network structures form during solidification in the Ce-modified Al–Zn–Mg–Cu alloy. This result is attributed to the large

number of Cu atoms trapped in Al_2(Cu, Ce) phase; therefore, Cu concentration in the final residual liquid is relatively lower. In addition, after homogenization, sufficient elimination of Al_2CuMg phase is achieved with 0.12 wt% Ce addition. This result is due to the large number of Cu atoms trapped in the stable AlCuCe phase and the formation of finer lamellar eutectic structures, which favor dissolution during homogenization.

Acknowledgements This study was financially supported by the Natural Science Foundation of Shandong Province, China (Nos. ZR2017PEM005 and ZR2017MEM005), the Project of Scientific Research Development of Shandong Universities China (Nos. J17KA043 and J17KB076), the Key Research Program of Shandong Province, China (No. 2015GGX102021), the Foundation for Applied Science and Technology Research and Development Program of Guangdong Province, China (No. 2015B090926007) and 2015 Shandong Province Project of Outstanding Subject Talent Group.

References

[1] Lu JT, Huang H, Wu H, Wen SP, Gao KY, Wu XL, Nie ZR. Mechanical properties and corrosion behavior of a new RRA--treated Al–Zn–Mg–Cu–Er–Zr alloy. Rare Met. 2017. https://doi.org/10.1007/s12598-017-0967-9.

[2] Liu JT, Zhang YA, Li XW, Li ZH, Xiong BQ, Zhang JS. Phases and microstructures of high Zn-containing Al–Zn–Mg–Cu alloys. Rare Met. 2016;35(5):380.

[3] Wen K, Xiong BQ, Fan YQ, Zhang YA, Li ZH, Li XW, Wang F, Liu HW. Transformation and dissolution of second phases during solution treatment of an Al–Zn–Mg–Cu alloy containing high zinc. Rare Met. 2018;37(5):376.

[4] Fan YQ, Wen K, Li ZH, Li XW, Zhang YA, Xiong BQ, Xie JX. Microstructure of as-extruded 7136 aluminum alloy and its evolution during solution treatment. Rare Met. 2017;36(4):256.

[5] Liu XY, Pan QL, Fan X, He YB, Li WB, Liang WJ. Microstructural evolution of Al–Cu–Mg–Ag alloy during homogenization. J Alloys Compd. 2009;484(1–2):790.

[6] Sharma Mala M. Microstructural and mechanical characterization of various modified 7XXX series spray formed alloys. Mater Charact. 2008;59(1):91.

[7] Robson JD. Microstructural evolution in aluminium alloy 7050 during processing. Mater Sci Eng A. 2004;382(1–2):112.

[8] Fan XG, Jiang DM, Meng QC, Zhong L. The microstructural evolution of an Al–Zn–Mg–Cu alloy during homogenization. Mater Lett. 2006;60(12):1475.

[9] Deng Y, Yin ZM, Cong FG. Intermetallic phase evolution of 7050 aluminum alloy during homogenization. Intermetallics. 2012;26:114.

[10] Liu Y, Jiang DM, Xie WL, Hu J, Ma BR. Solidification phases and their evolution during homogenization of a DC cast Al–8.35Zn–2.5Mg–2.25Cu alloy. Mater Charact. 2014;93:173.

[11] Zhang HH, Duan HL, Shao GJ, Xu LP, Yin JL, Yan B. Modification mechanism of cerium on the Al–18Si alloy. Rare Met. 2006;25(1):11.

[12] Chaubey AK, Mohapatra S, Jayasankar K, Pradhan SK, Satpati B, Sahay SS, Mishra BK, Mukherjee PS. Effect of cerium addition on microstructure and mechanical properties of Al–Zn–Mg–Cu alloy. Trans Indian Inst Met. 2009;62(6):539.

[13] Lai JP, Jiang RP, Liu HS, Dun XL, Li YF, Li XQ. Influence of cerium on microstructures and mechanical properties of Al–Zn–Mg–Cu alloys. J Cent South Univ Technol. 2012;19(4):869.

[14] Bo H, Jin S, Zhang LG, Chen XM, Chen HM, Liu LB, Zheng F, Jin ZP. Thermodynamic assessment of Al–Ce–Cu system. J Alloys Compd. 2009;484(1–2):286.

[15] Yu XX, Yin DF, Yu ZM, Zhang YR, Li SF. Effects of cerium addition on solidification behaviour and intermetallic structure of novel Al–Cu–Li alloys. Rare Metal Mater Eng. 2016;45(6):1423.

[16] Norman AF, Prangnel PB, Mcewen RS. The solidification behaviour of dilute aluminium–scandium alloys. Acta Mater. 1998;46(16):5715.

[17] Gao MC, Ünlü N, Shiflet GJ, Mihalkovic M, Widom M. Reassessment of Al–Ce and Al–Nd binary systems supported by critical experiments and first-principles energy calculations. Metall Mater Trans A. 2005;36(12):3269.

[18] Chen KH, Fang HC, Zhang Z, Huang LP. Effect of Yb additions on microstructures and properties of high strength Al–Zn–Mg–Cu–Zr alloys. Mater Sci Forum. 2007;546–549:1021.

[19] Wen SP, Xing ZB, Huang H, Li BL, Wang W, Nie ZR. The effect of erbium on the microstructure and mechanical properties of Al–Mg–Mn–Zr alloy. Mater Sci Eng A. 2009;516(1–2):42.

[20] Gazizov M, Teleshov V, Zakharov V, Kaibyshev R. Solidification behaviour and the effects of homogenisation on the structure of an Al–Cu–Mg–Ag–Sc alloy. J Alloys Compd. 2011;509(39):9497.

[21] Yu XX, Yin DF, Yu ZM, Zhang YR, Li SF. Microstructure evolution of novel Al–Cu–Li–Ce Alloys during homogenization. Rare Metal Mater Eng. 2016;45(7):1687.

[22] Mohanty PS, Gruzleski JE. Mechanism of grain refinement in aluminium. Acta Metall Mater. 1995;43(5):2001.

[23] Xiao DH, Huang BY. Effect of Yb addition on precipitation and microstructure of Al–Cu–Mg–Ag alloys. Trans Nonferrous Met Soc China. 2007;17(6):1181.

[24] Zolotorevsky VS, Belov NA, Glazoff MV. Casting Aluminum Alloys. 1st ed. Amsterdam: Elsevier; 2007. 8.

[25] Li H, Cao DH, Wang ZX, Zheng ZQ. High-pressure homogenization treatment of Al–Zn–Mg–Cu aluminum alloy. J Mater Sci. 2008;43(5):1583.

[26] Liu JT, Zhang YA, Li XW, Li ZH, Xiong BQ, Zhang JS. Thermodynamic calculation of high zinc-containing Al–Zn–Mg–Cu alloy. Trans Nonferrous Met Soc China. 2014;24(5):1481.

[27] Teng HT, Xiong BQ, Zhang YG, Liu HW, He X. Solidification microstructure of high zinc containing AlZnMgCu Alloys. Chin J Nonferrous Met. 2015;25(4):852.

[28] Seyed Ebrahimi SH, Emamy M, Pourkia N, Lashgari HR. The microstructure, hardness and tensile properties of a new super high strength aluminum alloy with Zr addition. Mater Des. 2010;31(9):4450.

[29] Cong FG, Zhao G, Jiang F, Tian N, Feng LR. Effect of homogenization treatment on microstructure and mechanical properties of DC cast 7X50 aluminum alloy. Trans Nonferrous Met Soc China. 2015;25(4):1027.

[30] Shu WX, Liu JC, Hou LG, Cui H, Liu JT, Zhang JS. Microstructural evolution of Al–8.59Zn–2.00Mg–2.44Cu during homogenization. Int J Miner Metall Mater. 2014;21(12):1215.

[31] Wang SH, Meng LG, Yang SJ, Fang CF, Hao H, Dai SL, Zhang XG. Microstructure of Al–Zn–Mg–Cu–Zr–0.5Er alloy under as-cast and homogenization conditions. Trans Nonferrous Met Soc China. 2011;21(7):1449.

[32] Hua C, Zhang YG, Li XW, Zhu BH, Wang F, Xiong BQ. Homogenizing treatment of Al–7.5Zn–1.6Mg–1.4Cu alloy. Chin J Rare Met. 2008;32(6):803.